Received: 2 August 2021 | Revised: 22 February 2022 | Accepted: 11 March 2022

DOI: 10.1049/rpg2.12455

IET Renewable Power Generation

The Institution of Engineering and Technology WILEY

ORIGINAL RESEARCH

Dynamic wake analysis of a wind turbine providing frequency support services

Narender Singh[1,2] | **Jeroen D. M. De Kooning**[1,3] | **Lieven Vandevelde**[1,2]

[1]Department of Electromechanical, Systems and Metal Engineering, Ghent University, Ghent, Belgium

[2]FlandersMake@UGent - Core lab EEDT-DC, Flanders Make, Belgium

[3]FlandersMake@UGent - Core lab EEDT-MP, Flanders Make, Belgium

Correspondence
Narender Singh, Department of Electromechanical, Systems and Metal Engineering, Ghent University, Ghent, Belgium.
Email: narender.singh@ugent.be

Funding information
BEOWIND project is funded by Energy transition fund of the Belgian Federal government

Abstract

The participation of wind farms in providing ancillary services is an asset for the power system and one way to maintain a strong grid with the increasing penetration of renewable energy sources. Research has shown this to be feasible for wind farms by using efficient prediction and sophisticated control systems. In some parts of the world, strict grid codes are already being implemented that require wind farms to provide ancillary services. Moreover, the primary reserve market in Europe is moving towards shorter procurement periods, providing wind farms an opportunity to more efficiently optimise their resources based on short term forecasts. It can however be challenging for the wind farms to efficiently participate in grid frequency support services, especially for primary reserve services. The reason behind this is the requirement of quick activation and deactivation of power reserve margin for services such as Frequency Containment Reserve (FCR) and Fast Frequency Response (FFR). A full activation of the contracted reserve is required within seconds of a grid frequency dip. A sudden change in wind turbine dynamics is expected to have an impact on the wake behind the wind turbine. The wake effect within a wind farm is taken into thorough consideration in its design process. The effect on the wake due to the wind turbines participating in fast response ancillary services however, remains unexplored. This is a matter of greater concern for wind farms with a high capacity density. To this end, the main contribution of this article is to observe the effect of ancillary service based control system on the wake effect of a wind turbine. Additionally, the capability of developed wind turbines controllers to follow primary reserve services are also tested. FFR and FCR services are tested for a range of frequency designs, these include both synthetic and actual grid frequencies. The synthetic frequency profiles are designed to replicate both fast and slow frequency variations in order to analyse the impact on wake behaviour. The simulations are performed for low and high wind speed including constant as well as turbulent winds.

1 | INTRODUCTION

In line with the European Union (EU) target for 2050 to reduce greenhouse gas emissions to 80–95% below the 1990 levels [1], the power systems all over Europe see an increasing renewable energy penetration every year. In 2019, Europe added 15.4 GW of new wind power capacity. This adds up to a total of 205 GW of installed wind energy capacity in Europe. In 2019, 15% of the total electricity consumed by all EU-nations was generated by using wind energy [2]. The worldwide wind power capacity is 743 GW, with 93 GW of new installed capacity in 2020 [3]. As the share of wind energy increases in the power mix, it is naturally expected that wind farms provide ancillary services. In some areas of the world, strict grid codes are already being implemented that require wind farms to provide ancillary services [4]. Transmission system operators (TSO) in various countries offer the opportunities for production units to participate in the primary reserve market. Some of these services include frequency containment reserve (FCR), fast frequency response (FFR), synchronous inertial response (SIR), enhanced

frequency response (EFR), fast post-fault active power recovery (FPFAPR), etc.

Participation in these reserve markets is strictly based on the ability of a production unit to increase or decrease the reserve power within a fixed span of time. Usually this time range is very small ranging from an instantaneous response to a few seconds. In order to qualify to participate in these markets, the production units need to prove their ability to efficiently provide these services by going through several tests. Providing these services is a challenge for production units that are fully converter-interfaced, such as a wind farm. A support from energy storage technologies such as supercapacitors, flywheels, batteries etc., can be sought in such cases [5], [6]. These technologies can provide desired active power output within 0.5–2 s [7]. However, many power system operators in Europe forbid the participation of energy storage power plants in the primary reserve market [8]. New control systems for wind turbines are potentially capable of a quick response to the changing grid frequency. Hence, this makes them an eligible candidate for frequency support ancillary services. Studies have shown the feasibility and methods of operating wind farms as FCR and FFR provider [9–16].

Regarding wind turbine control, several different techniques are available [17–19]. A generator control method that uses direct torque control (DTC) for an interior mounted magnet PMSG is presented in [20]. An improved direct torque control method for smooth power injection and short circuit protection is presented in [21]. These control strategies are widely used for variable-speed generation and for extracting the maximum power available in the wind. The conventional operation of a wind turbine is to use maximum power point tracking (MPPT) to extract maximum power or power limiting control (PLC) in case of wind speeds higher than the rated wind speed. However, the control system required for this study should not only operate in MPPT and PLC, but should also be able to follow the reference power signal that changes with the fast varying input grid frequency. The results from this research supports the effectiveness of fast frequency response from wind turbine control on supporting active power disturbances in low-inertia power systems. An added advantage for wind farms in this scenario is that the FCR market in Europe is moving towards shorter procurement periods [22], [23]. Since the wind prediction is more reliable and accurate on short time scale, it is easier for wind farms to make a more confident bid in the FCR market.

In order to provide ancillary services with a wind turbine, its power output must vary more dynamically, especially when providing short-term grid balancing services such as inertial response, FCR and FFR. However, these dynamic power variations impact the wake effect, which in turn could impact neighbouring turbines. The study of wake effects is even more significant for wind farms with high capacity density. Countries like Belgium and Germany have higher capacity densities of offshore wind farms as compared to the European average. The reason for this high density in Belgium is the regulatory framework. Due to the limited space resources in the Belgian North Sea, the obligated policy demands the use of space granted as intensively as possible [24].

The wind farms located in close proximity generate wake effects that reduce the downwind wind speeds. Studies have shown that these effects can extend over 50 km resulting in economic losses for the wind farms owners [25]. Methods have been developed in order to minimise the impact of the wake and optimise the wind farm power output. These methods use algorithms developed to maximise the annual energy production (AEP) of wind farms [26]. One such approach utilises optimised yaw alignment that deflects wakes away from downstream turbines and wind farms [27]. Such measures have shown to improve the wind speed by up to 13%. Studies have been conducted to demonstrate the significance of wake effects in influencing the inertial response capacity of a wind farm [28]. However, a research gap is seen for studies on wake effects produced by wind turbines providing FCR and FFR.

To this end, the scope of this paper lies in the study of dynamic wake behaviour of a wind turbine providing FCR and FFR. The study presented in this paper uses a detailed wind turbine model to simulate FCR and FFR based control. The influence of the control strategy on the wake behind the turbine at several locations behind the wind turbine is observed. The model uses a conventional proportional-integral (PI) controller to generate blade pitch commands. The torque is controlled by a grid frequency following algorithm. A reference power is generated based on the frequency and the power output is adjusted accordingly. Different frequency profile designs have been used in the presented simulations.

The article is organised as follows: Section 2 presents the models used for the simulations in this study. The two ancillary services investigated in the article are discussed in Section 3. The frequency and wind inputs to the model are presented in Section 4. The different control systems used in this study are presented in Section 5. The tests performed and the results from this study are presented in Section 6. Discussion and conclusions are drawn in Section 7.

2 | MODEL DESCRIPTION

The simulation setup consists of a wind turbine model in FAST, a generator model and the control system in MATLAB Simulink. These models are interconnected as a co-simulation with loop communications at each time-step of the simulation. Additionally, the data is post-processed using a wake model.

2.1 | Wind turbine

The wind turbine model used in the simulations is the NREL 5 MW baseline wind turbine. This model has been implemented in FAST by NREL, a tool for simulating the coupled dynamic response of wind turbines. This elaborate software combines aerodynamic, hydrodynamic, structural and electrical system models of different types of wind turbines. The main model properties are listed in Table 1 [29]. The power curve of this turbine is presented in Figure 1.

TABLE 1 Wind turbine properties

Property	Specification
Power rating	5 MW
Rotor orientation & configuration	Upwind, 3 blades
Rotor and hub diameter	126 m and 3 m
Hub height	90 m
Cut-in, Rated and Cut-out wind speed	3.0 m/s, 11.4 m/s and 25.0 m/s

TABLE 2 Generator properties

Property	Specification
Rated power	5 MW
Rated speed	12.1 rpm
Efficiency	93%
Pole pairs	117
Nominal voltage	1950 V
Nominal current	876 A
R_c, R_s, L_q	77.34 Ω, 98.5 mΩ, 5.86 mH

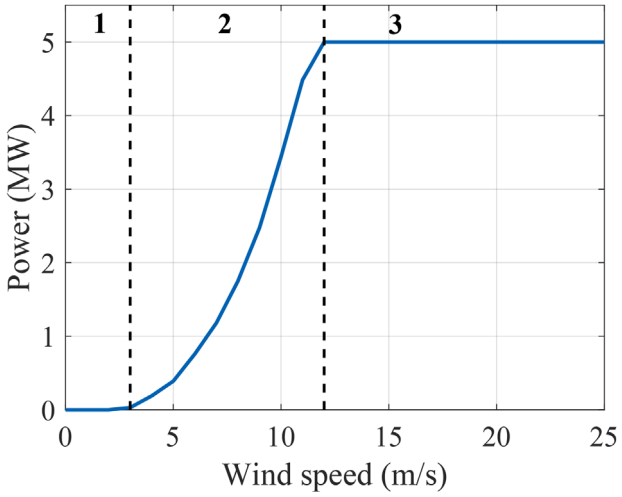

FIGURE 1 Power curve of 5 MW wind turbine

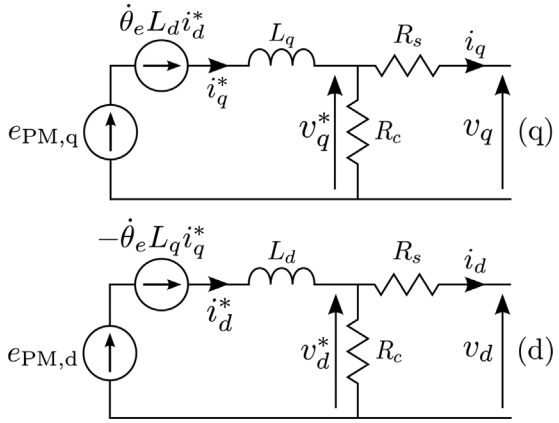

FIGURE 2 Equivalent diagram of a PMSG in the rotating reference frame

The operation range of the wind turbine is divided into three different regions based on the wind speed, as shown in Figure 1. In Region 1, the wind speed is below the cut-in speed, thus the torque is zero and no power is extracted. In Region 2, the power is classically optimized by means of MPPT control. In Region 3, the wind speed is above the nominal value of 11.4 m/s. There, the torque, speed and power are limited to their respective rated values to avoid overloading the drivetrain components.

2.2 | Generator

The generator model used in this study is a Permanent Magnet Synchronous Generator (PMSG). The main properties of the generator are listed in Table 2. The equivalent diagram of the generator is presented in Figure 2. The generator is modeled in the rotating (d,q) rotating reference frame. In Figure 2, $e_{PM,q}$ is the permanent magnet induced back-emf voltage, which is proportional to the rotor speed. The d and q equivalents also consist of an additional back-emf each proportional to the current in the other scheme due to the armature reaction effect. R_s and R_c, respectively, represent the copper losses in the stator winding and the iron losses.

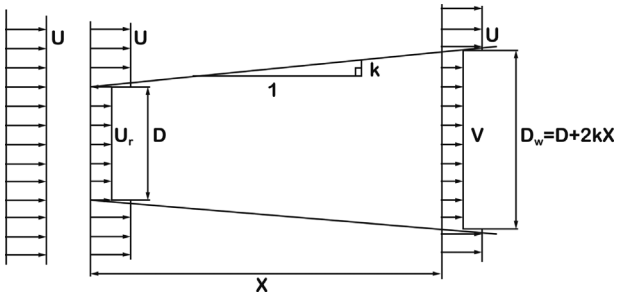

FIGURE 3 Wake schematic

2.3 | Wake model

The Jensen wake model is one of the oldest and most popular models used in wake studies [30]. It is a simple model to analyse the wake effect. In its original form, it does not account for the wind turbine dynamics. However, for this study, a robust yet computationally simple wake model that accounts for wind turbine dynamics was required. Therefore a modified Jensen model, that is, Jensen-Katic, is used in this study [31]. This model allows to incorporate the actual characteristics of the turbine, thus different control behaviours of the machine can be modelled. Figure 3 schematically shows the wake. The free flow ambient speed is denoted by U. The wake behind the turbine is

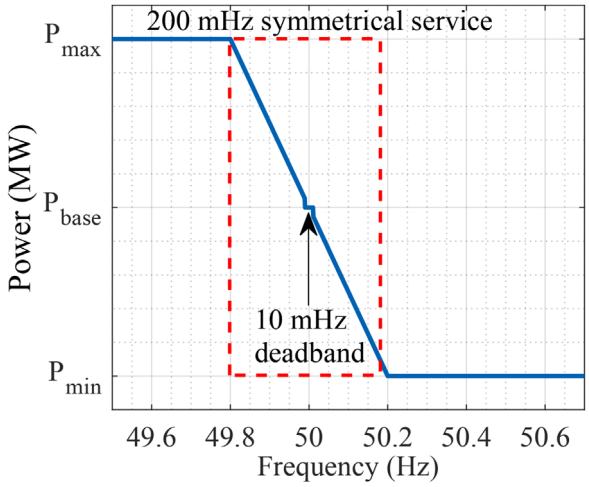

FIGURE 4 200 mHz symmetrical service

assumed to have an initial diameter equal to the rotor diameter D. The wake diameter at a distance X is defined as D_w. The velocity deficit V at a given distance X depends on the thrust coefficient c_t, and is defined as:

$$V = U\left(1 - \frac{1 - \sqrt{1 - c_t}}{\left(1 + \frac{2kX}{D}\right)^2}\right). \quad (1)$$

3 | ANCILLARY SERVICES

A range of different ancillary services are offered for production units by TSOs in different countries. In this research two kinds of primary reserve ancillary services are tested. This section gives a brief overview of these services.

3.1 | Frequency containment reserve

The Belgian TSO Elia procures grid frequency balancing services through two different frameworks based on the generation capacity of the production units. These contracts are the Contract for the Injection of Production Units (CIPU) and non-CIPU. For harmonisation of FCR products and FCR procurement rules on the European level, from July 2020 on, only the 200 mHz symmetrical service are continued [32]. Due to this reason, the FCR tests presented in this work are conducted for a 200 mHz symmetrical service. In this type of service, a proportional frequency support within the range of 49.8–50.2 Hz of grid frequency is required from the participating production unit.

The relation between the reference power and the grid frequency for a 200 mHz symmetrical service can be seen in Figure 4. In this representation, the wind turbine operates at a base power P_{base}. With the change in grid frequency, the reference power follows a linear slope between P_{min} and P_{max}. The service is obligated between the bounds of 49.8–50.2 Hz. However unlikely, if the frequency drops or increases beyond this range, the power supply should be maintained at a constant, on upper or lower limit, respectively. A frequency response deadband of 10 mHz centred at nominal frequency (50 Hz) is present to reduce excessive controller activities and turbine mechanical wear for normal power system frequency variations.

TABLE 3 Type of FFR services

Type	Activation level [Hz]	Maximum full activation time [s]
A	49.7	1.3
B	49.6	1.0
C	49.5	0.7

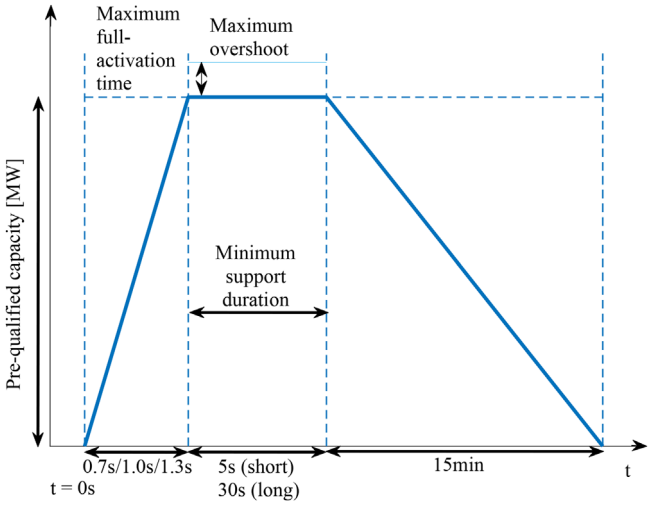

FIGURE 5 FFR framework

3.2 | Fast frequency reserve

The fast frequency response service has been adopted by different countries and therefore exists in various forms and manners. For the tests presented in this research, FFR as defined for the Nordic synchronous area was chosen [33]. All the generation units intending to participate in the FFR market must pass a prequalification process to ensure their ability to deliver FFR when ordered by the TSO. A crucial part of this prequalification process is a prequalification test. The specified support durations are, 'long support duration FFR' (at least 30 s) and 'short support duration FFR' (at least 5 s). There are 3 different combinations of FFR services available that can be freely chosen by the production units. These services presented in Table 3 differ in activation level and the required maximum activation level.

The participants are free to choose from the type of service they intend to provide beforehand. Figure 5 is a graphical

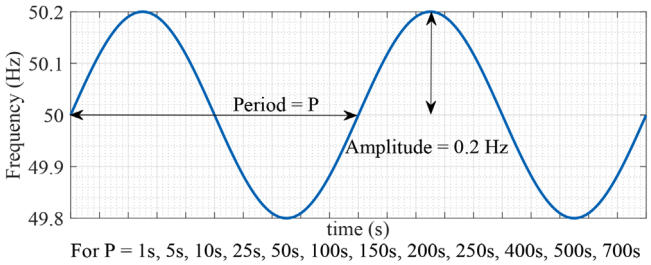

FIGURE 6 Frequency with sinusoidal ripples

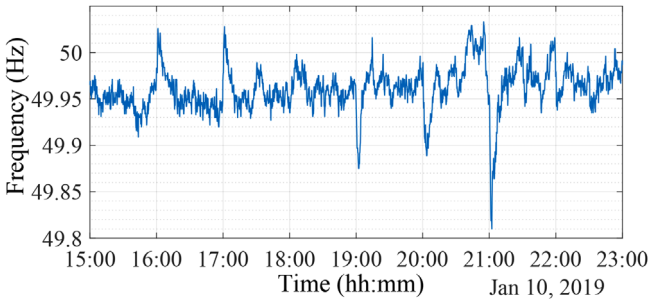

FIGURE 7 Frequency data extreme event

representation of the FFR service. The activation instant at $t = 0$ s is the moment when the FFR reserve is activated. Depending on the type of service chosen by the production unit, an upper time limit ranging from 0.7 s to 1.3 s is given during which the full activation should be completed. The activation level should be sustained for the minimum support duration based on the choice of long duration or short duration support. At the end of the support duration the production units are given a recovery time of 15 min, after which the production units must be fully prepared for a new support cycle. During the support duration a maximum overshoot equivalent to 35% of the prequalified FFR capacity is permissible.

4 | DATA

The simulations presented in this study require two essential datasets. The developed FCR and FFR based control models require a frequency input on every time step. Additionally, to be able to run a wind turbine model in FAST, a fitting wind field model is necessary.

4.1 | Frequency data

The simulations performed for FCR services in this work are performed for different frequency profiles. These data form an important input for the controller as it determines the reference power for the frequency following controller. The first frequency dataset is an artificially generated frequency pattern with a sinusoidal ripple, with an amplitude of 0.2 Hz and 12 different periods of 1 s, 5 s, 10 s, 25 s, 50 s, 100 s, 150 s, 200 s, 250 s, 400 s, 500 s and 700 s, respectively. Figure 6 shows a sample of these data. The frequency is sampled at the same rate as the time step of simulations. This artificial frequency is used to investigate the propagation of FCR dynamics in the wake. Moreover, by simulating the different scenarios with varying frequency of oscillation, the aim is to assess the varying magnitude of propagation in the wake.

The second frequency dataset is actual grid frequency dataset of the European synchronous grid. The frequency retrieved from the source is sampled every 0.5 s [34]. However, to adjust the frequency to the simulation time-step, the frequency data are interpolated. Figure 7 presents a section of frequency data used in the simulations. The frequency data are from an extreme

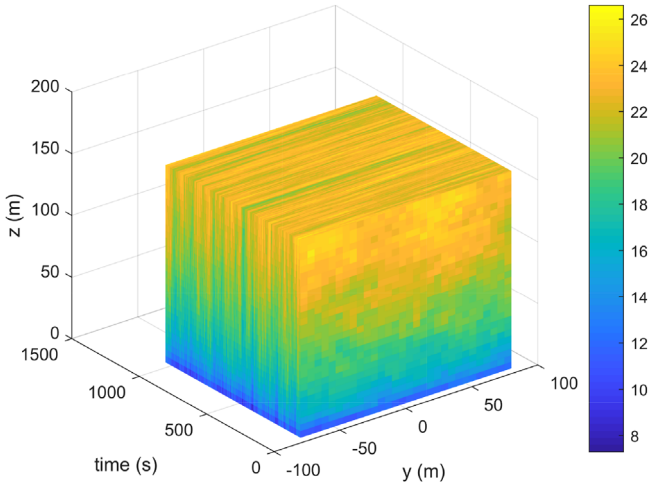

FIGURE 8 u-component of wind speed (m/s)

event that occurred on the 10 January 2019, 21:02 CET. During this event, the continental European power system stretching across 26 countries witnessed the largest absolute frequency deviation since 2006 [35]. During this rare event, the frequency dropped to 49.8 Hz. The reason for choosing this event is to clearly observe the impact of changing grid frequency on a turbine providing FCR.

4.2 | Wind field

In FAST, different wind profile input methods are available and can be used for analysis. For the simulations performed in this study two different wind profiles are used. These are presented in the following.

4.2.1 | Constant wind field

In the simulations presented in this work, steady wind profiles of 7 m/s and 12 m/s is used. These wind speeds are chosen to study the behaviour of the wake in both low and high winds, respectively.

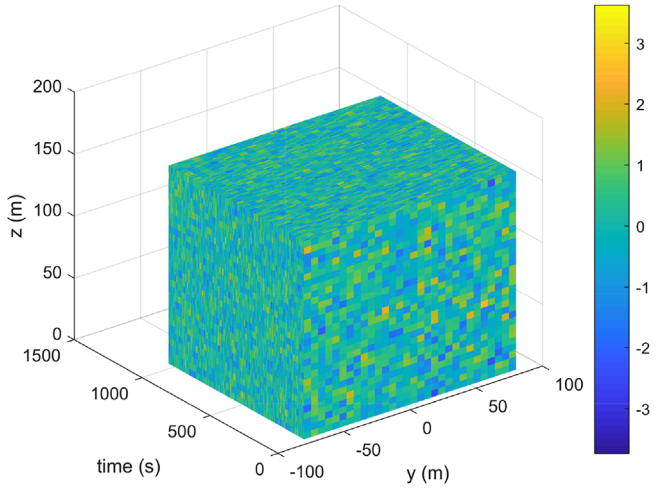

FIGURE 9 v-component of wind speed (m/s)

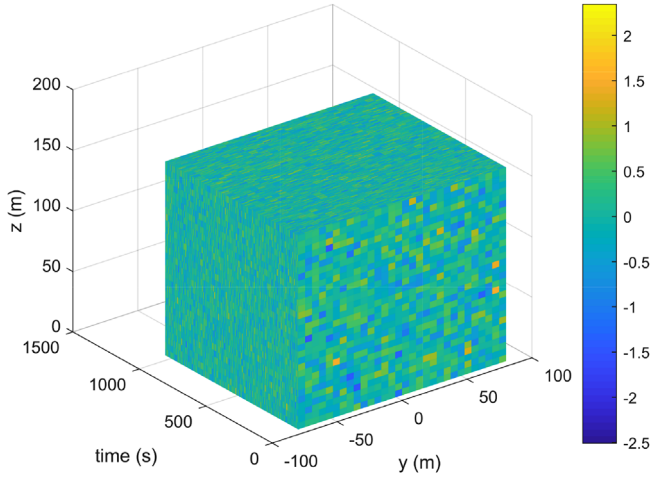

FIGURE 10 w-component of wind speed (m/s)

4.2.2 | Turbulent wind field

A three-dimensional turbulent wind field is used to analyse the wake effect of a wind turbine providing frequency support. The TurbSim Risø smooth-terrain model (SMOOTH) based on [36] and [37] is used to generate the turbulent wind data. The wind field has a grid height and width of 160 m. The three components of the wind field are presented in Figures 8, 9 and 10. The inertial reference frame of these three components: The u-component is along the positive X-axis (downwind). The v-component is along positive Y-axis (to the left when looking along X). The w-component up, along positive Z-axis (opposite gravity.) The reference height of the wind field is chosen similar to the height of the wind turbine rotor hub at 90 m. The mean wind speed is 20 m/s and the turbulence intensity is 5%. The wind speed values within the simulated time ranges from 16.45 m/s to 23.1 m/s.

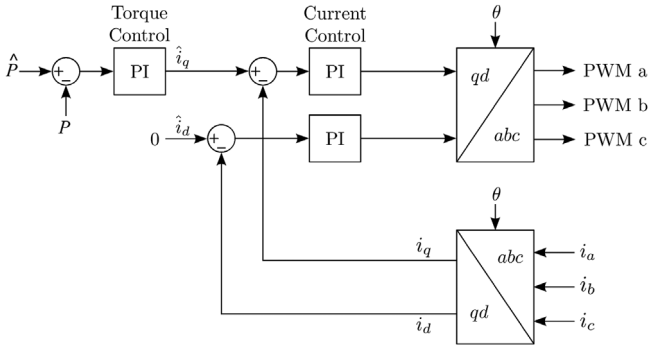

FIGURE 11 Field oriented control

5 | CONTROL

Field oriented control (FOC) is selected for the torque control of the PMSG. In this control method, the direct current component is regulated to zero and the quadrature current is proportional to the torque. Figure 11 shows the field oriented control schematically. The control system is a PI controller that generates a current signal based on a comparison between the reference power value and the actual power output from the generator at each time step. The reference power that serves as an input to the controller is a time varying signal generated as per the requirement of the prequalification test. The value of the reference power is defined by the grid frequency. The PI controller is optimized in a manner such that the tracking error is minimized by minimizing overshoot and settling time. The controller is tested under different wind conditions, ranging from highly turbulent wind conditions to steady wind. The performance of the controller varies depending on several factors such as the wind conditions and the rate of change of reference power.

5.1 | FCR control

The maximum available power P_{max} that can be harnessed by the turbine is dependent on the wind speed and is defined by the power curve as presented in Figure 1. In order to provide an FCR reserve power P_{FCR} equivalent to 20% of P_{max}, the wind turbine is operated at a base power equal to 80% of P_{max}. The turbine ramps up and down within 60% to 100% of P_{max} based on the grid frequency. In this manner, there is enough capacity at all times to follow the grid frequency in the specified range. The control algorithm to generate the reference power based on the grid frequency is defined in Algorithm 1.

Figure 12 shows the generator power under PLC and FCR based controls. The generated power is plotted on the left y-axis and the grid frequency on the right y-axis. The case considered here has a steady wind speed input of 12 m/s. It can be seen that the power output under PLC control is constant at 5 MW, whereas, with FCR control, the generator power varies with the changing grid frequency. The effect of changing grid frequency can be seen on the power output. The controller works

ALGORITHM 1 Reference power decision

Require: $P_{\max} \geq P_{\text{ref}}$
  if $f \leq 49.8\ Hz$ **then**
    $P_{\text{ref}}(t) = P_{\max}$
  else if $49.80Hz < f < 49.99\ Hz$ **then**
    $P_{\text{ref}}(t) = P_{\max} + (50.80 - f)$
  else if $49.99Hz < f < 50.01Hz$ **then**
    $P_{\text{ref}}(t) = P_{\max} - P_{\text{FCR}}$ ▷ $10mHz$ deadband
  else if $50.01Hz < f < 50.20Hz$ **then**
    $P_{\text{ref}}(t) = P_{\max}(50.80 - f)$
  else if $f > 50.20Hz$ **then**
    $0.6\ P_{\max}$
  end if

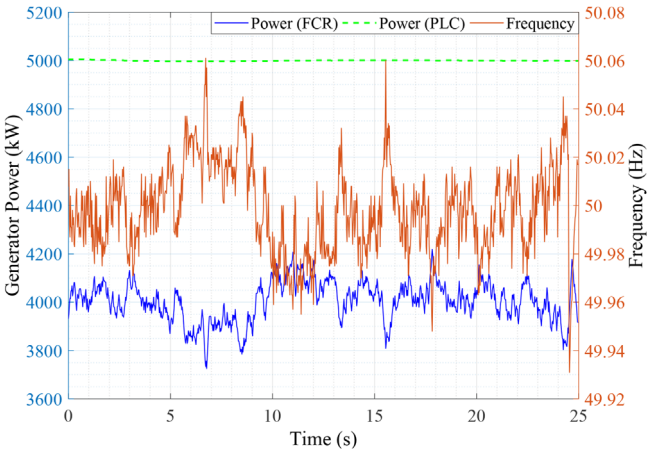

FIGURE 12 Generator PLC and FCR power

with a satisfactory tracking performance, following the reference power with low error.

5.2 | FFR Control

There are three different types of FFR services as presented in Table 3. These service require a fast response time to adjust the power output to the changing grid frequency. As a result, the controller presented in Section 5.1, in its current form is unable to follow these rapid variations in the reference power signal. Therefore, the simulations for FFR service are performed in FAST.Farm.

There is no control method in Fast.Farm that can include the effect of changing grid frequency on the power output of a wind turbine providing frequency support services. The sole control option is the torque control built within the program. For this reason, the control system in FAST.Farm has been modified to operate the turbine with FFR based control.

The operation is modified such that instead of providing a constant power, the power output is based on the changing input grid frequency. This control is defined in the following

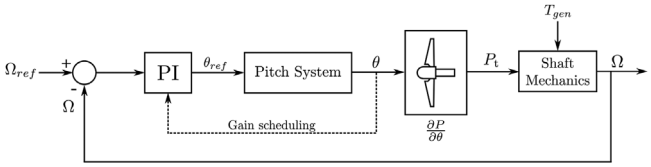

FIGURE 13 Pitch control

equations:

$$P_{\text{ref}} = P_{\text{base}} + P_{\text{freq}}(t), \tag{2}$$

where,

$$P_{\text{freq}} = (50.8 - f)P_{\text{FCR}}. \tag{3}$$

Here, the reference power P_{ref} is calculated as the sum of base power P_{base} and a time varying term $P_{\text{freq}}(t)$. Furthermore, $P_{\text{freq}}(t)$ is defined by the changing grid frequency and the contracted FCR bid P_{FCR}.

5.3 | Pitch control

The simulations presented in this study also consist of wind turbine operation for wind speeds higher than the rated speed. Therefore, a pitch control system is required. The pitch control system is developed in MATLAB Simulink and is inter-linked with the wind turbine model in FAST. The block diagram of the pitch control system is presented in Figure 13. A PI controller has a gain-scheduling input and compares the reference rotor speed $\boldsymbol{\Omega}_{\text{ref}}$ to the actual rotor speed $\boldsymbol{\Omega}$. Based on the error, a control signal is generated at each time-step and is sent to the wind turbine model in FAST.

For the simulations performed in FAST.Farm, the baseline blade-pitch controller has been used. The controller is activated in the region of control where the wind speed exceeds the rated wind speed. The commands from this controller are computed by using gain scheduling PI control on the speed error between the generator speed and the rated generator speed [29].

6 | RESULTS AND DISCUSSION

Using the aforementioned data, models and control systems, several tests are performed for different wind profiles and frequencies to analyse the dynamic impact of ancillary service provision on the turbine wake. This section presents the results of these simulations in the form of 4 case studies:

I. FCR provision with oscillating grid frequency
II. FCR provision with realistic grid frequency
III. FCR provision in turbulent wind
IV. FFR provision of Types A, B and C

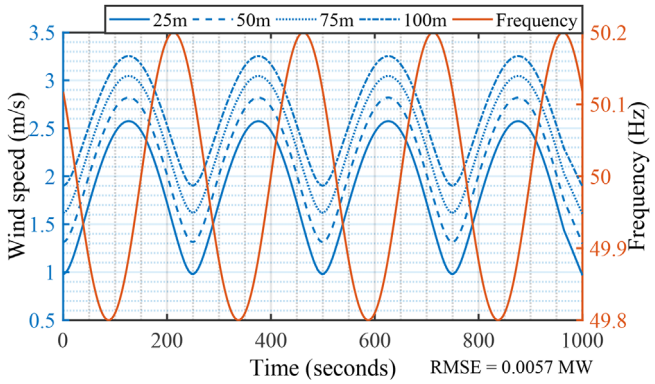

FIGURE 14 Wind speed at different points behind the rotor for 7 m/s simulations

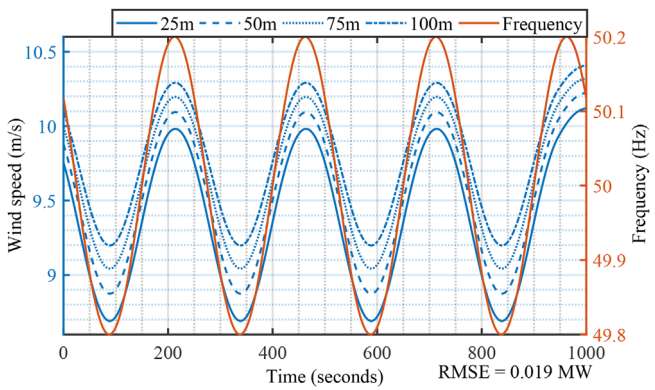

FIGURE 15 Wind speed at different points behind the rotor for 12 m/s simulations

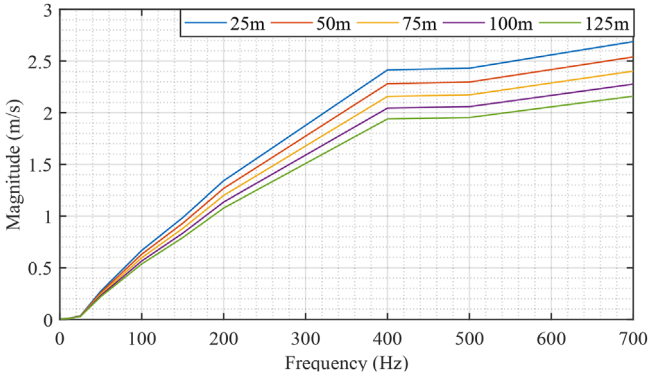

FIGURE 16 Magnitude of wake oscillations with period varying grid frequency for 7 m/s simulations

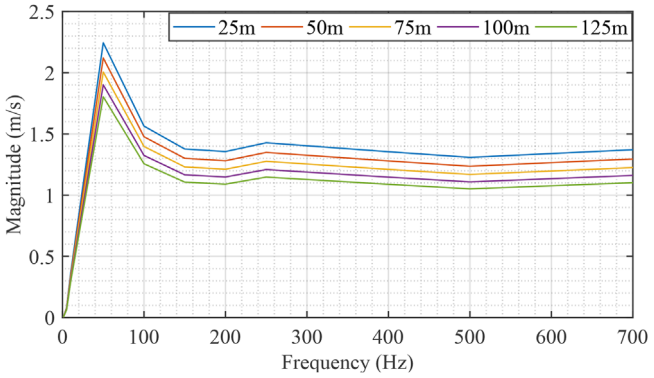

FIGURE 17 Magnitude of wake oscillations with period varying grid frequency for 12 m/s simulations

6.1 | Case I: FCR provision with oscillating grid frequency

In case study I, the wind turbine is subjected to steady wind fields of 7 m/s and 12 m/s, respectively. An artificial grid frequency dataset is generated which contains sinusoidally varying ripples, as presented in Section 4.1. Although such an oscillating grid frequency does not occur in practice, it is used here to achieve a clear understanding of how FCR provision dynamically impacts the wake. This will provide the required insight to study the dynamic impact of FCR on the wake for realistic grid frequency in case study II.

A series of 12 simulations with varying period of input grid frequency as presented in Figure 6 have been performed. The artificial sinusoidal frequency dataset is simulated to study how the dynamics in FCR propagate into the wake dynamics. To analyse the wake behaviour, several different points are chosen.

Figures 14 and 15 present the results from the simulation where the period of input grid frequency is 250 s for the cases with steady wind of 7 m/s and 12 m/s, respectively. In these figures, there are 4 blue curves corresponding to the left y-axis. These curves represent the wind speed at distances 25 m, 50 m, 75 m and 100 m horizontally behind the rotor center-line, respectively. The grid frequency is shown on the right y-axis. A very clear observation from these results is that the oscillations in the grid frequency are replicated in the wake behind the wind turbine. It can also be observed that the wind speed is most deteriorated at the point closest to the wind turbine and the effect gradually decreases as the distance from the wind turbine increases.

A series of 12 simulations with varying period of grid frequency were performed with the aim to observe the changing magnitude of wake with slow as well as fast variations in the grid frequency and thereby observing the varying magnitude of propagation in the wake. Figures 16 and 17 present these results at 5 different points for the steady wind cases of 7 m/s and 12 m/s, respectively. The x-axis shows the different periods of oscillations for which the simulations are performed. The y-axis shows the magnitude of oscillations in the wind speed at the specified points. A common observation drawn from these figures is that for a fast changing grid frequency with period <= 5 s, the oscillations are not replicated in the wake behaviour and no similar sinusoidal pattern is observed. As the period of oscillations increases, the input grid frequency behaviour starts to replicate in the wake. It can be seen in Figure 16 that there is a continuous increasing trend in the magnitude of wake for the frequencies with longer periods. However, the increment in magnitude is not continuously linear. On the other hand for the case of high wind speed, in Figure 17, a different pattern is

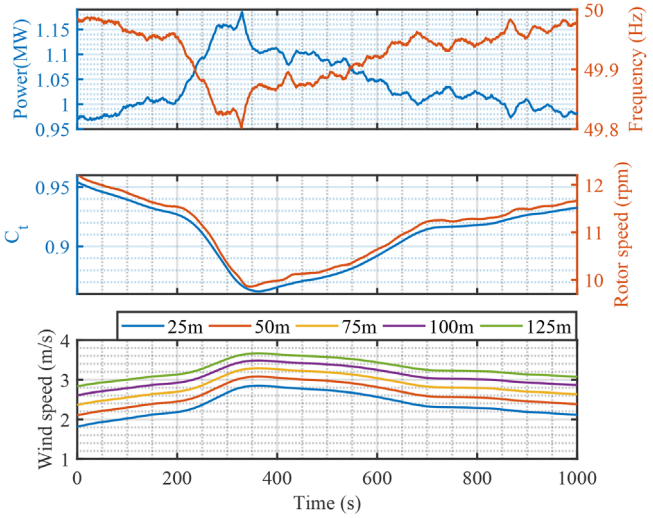

FIGURE 18 Grid frequency and influenced outputs with changing control action for a wind speed of 7 m/s

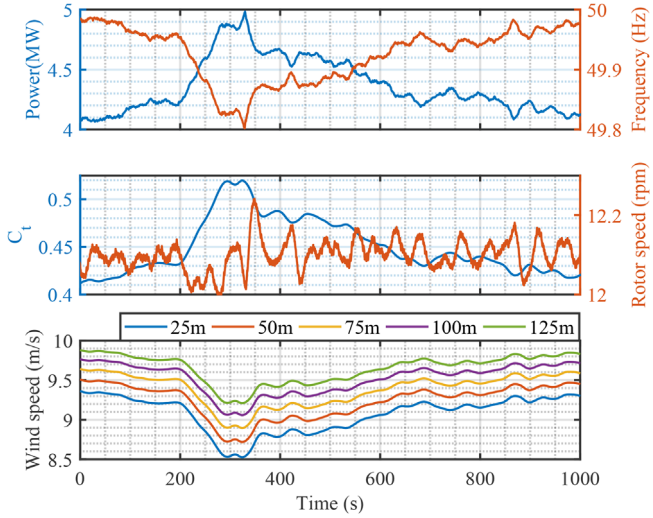

FIGURE 19 Grid frequency and influenced outputs with changing control action for a wind speed of 12 m/s

observed. The curves start with a steep slope and then gradually declines to a more stable wake magnitude.

6.2 | Case II: FCR provision with realistic grid frequency

To simulate a realistic scenario, real grid frequency data as shown in Figure 7 are used. In this case the wind turbine is subjected to steady wind profiles of 7 m/s and 12 m/s, as presented in Section 4.2.1. In order to study the wake effect in a realistic grid frequency condition, several physical points behind the rotor center-line have been chosen. These points are located at distances of 25 m, 50 m, 75 m, 100 m and 125 m behind the rotor. Figure 18 presents three different graphs resulting from simulations with a steady wind speed of 7 m/s. The first graph shows the output power with the varying grid frequency. The second graph shows the thrust coefficient C_t and the rotor speed. The third graph shows the wind speed at different points behind the rotor. During the extreme grid event, the grid frequency drops to 49.8 Hz. In response to this frequency dip, the controller generated a reference power to match the contracted FCR bid. The resulting control can be observed by comparing the blue and red curve. It can also be seen that the C_t and the rotor speed also drop at this point. The effect of this event can be seen on the wind speed at different points behind the rotor. At ≈ 400 s, an increase in the wind speed can be observed at each of these points.

Figure 19 present the graphs for the case where a steady wind speed of 12 m/s is used. The plot design and placement is similar to Figure 18. Here, the control response is again reflected on the output power. The rotor speed in this case sees little variation during this event. This is attributed to the pitch control action that was not active in the case of 7 m/s simulations. However, due to the control action, a changing wind speed at the points of observation is noticed. This change in the wind speed due to the wake behaviour although clearly noticeable, is rather minimal.

6.3 | Case III: FCR provision in turbulent wind

Case III studies the frequency support service in a turbulent wind field. The turbulent wind profile presented in Section 4.2.2 is used for these simulations. An 800 s simulation is performed for two different sub-cases. The first case is where the wind turbine operates with FCR based control. A percentage control is used such that the wind turbine provides a linear frequency support of 20% of its total capacity of 5 MW within the range of 49.8 Hz - 50 Hz. The second sub-case is without FCR and represents normal operation as a reference. The grid frequency is designed in a step form and ranges from 49.8-50 Hz within the span of the total simulation time.

The first graph in Figure 20 is the grid frequency that is used to calculate the reference power. The following 3 graphs consist of 2 curves. The FCR case is represented by a blue curve and the non-FCR case is represented by a red curve. It can be seen in the second graph that during this turbulent wind scenario, for the non-FCR case, the controller tries to follow the reference power of 5 MW. The root mean square error (RMSE) of the power reference tracking for this case is 0.0275 MW. On the other hand, the *blue* curve that represents the FCR power tries to follow the input frequency. The RMSE in this case is 0.0625 MW expectantly higher than the former case due to the increased control action. The third graph shows the C_t for two case. The C_t for both cases is identical, except for the duration in which the wind turbine provides FCR support. The fourth curve shows V_s, the wind speed for the two cases at a distance of 25 m behind and in centre-line of the rotor. The two wind speeds appear to differ slightly within the frequency support duration. To analyse this in more detail, the final graph shows

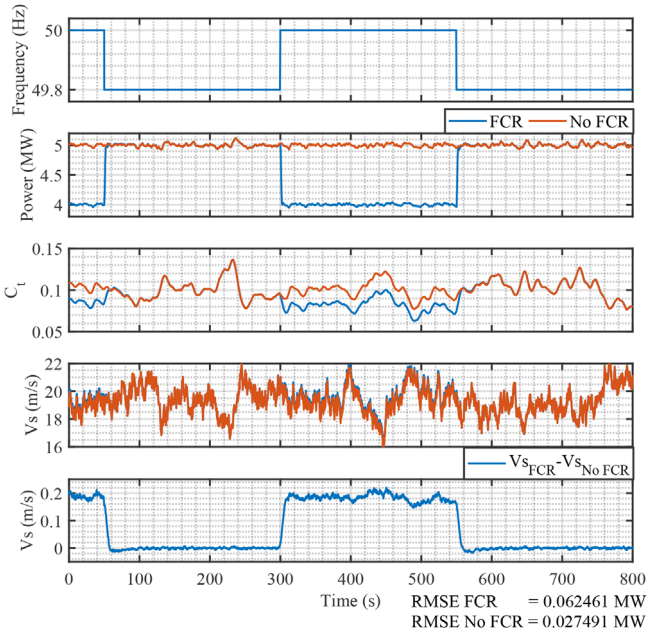

FIGURE 20 Case III: FCR provision in turbulent wind

the difference between the two wind speeds, $V_{s_{FCR}} - V_{s_{NoFCR}}$. It is evident that the wake effect indeed differs in the two cases.

6.4 | Case IV: FFR provision of types A, B and C

The prequalification test for FFR is designed such that all three types of services presented in Table 3 can be implemented. Initially there is a sequential step decrease in grid frequency to simulate a situation where all three types of services need to be activated. After this the services are individually activated from a stable grid frequency of 50 Hz. All the services are tested for a long duration support (> 30 s). The purpose of this test is to analyse the capacity of the wind turbine and control system to provide the FFR service. This test is presented in Figure 21.

The wind turbine provides 0.5 MW of FFR for Type A service and 0.25 MW each for Type B and Type C service. The red curve indicates the grid frequency. The frequency starts at a stable 50 Hz for the first 50 s, during this time, after the initial transient the wind turbine generates 4 MW of power retaining 1 MW for the FFR services. At time t = 50 s the frequency drops to 49.7 Hz and the Type A FFR service is activated and continues for the next 50 s. During this time the wind turbine generates 4.5 MW power. At time t = 100 s there is a further drop in the grid frequency to 49.6 Hz. At this moment the Type B service is activated and the total power output is increased by 0.25 MW to 4.75 MW. At time t = 150 s, Type C service is activated when the frequency drops to 49.5 Hz. The power output at this point is equal to the maximum power output of 5 MW. At time t = 200 s, the frequency is stabilised again at 50 Hz. At time t = 250 s the frequency drops again to 49.6 Hz, hence activating the Type B service. At time t = 350 s the frequency drops to 49.5 Hz and

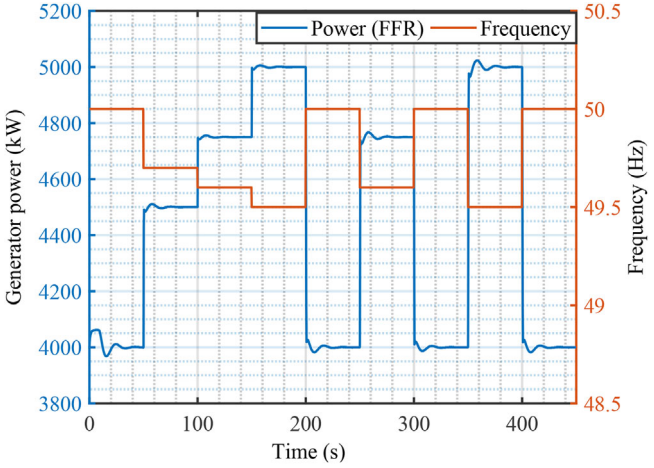

FIGURE 21 FFR power output and frequency

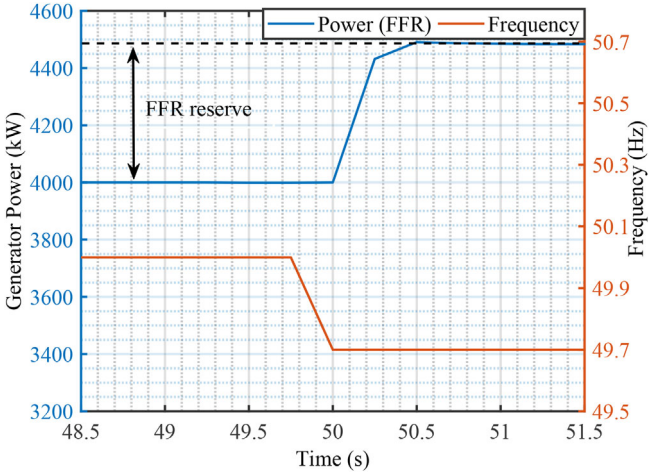

FIGURE 22 FFR Type A service

Type C service is activated. Figures 22–24 show the zoomed version of activation of all three services. From Figure 22 it can be seen that the Type A service is activated at t = 50 s and the FFR level of 0.5 MW is activated within 0.5 s.

Figure 23 shows the activation of the Type B service. In this case the FFR reserve of 0.25 MW is activated within the time limit of 1 s. At the instant of t = 150 s, the frequency drops to 49.5 Hz at this point the last 0.25 MW of reserve power is to be activated. However as can be seen in Figure 24, the controller was not able to activate the Type C service within the given time limit of 0.7 s. A possible reason for this is that at this instant the wind turbine is reaching the upper limit of its power output. A solution to this problem could be to reduce the reserve capacity of Type C service. D1, D2 and D3 are three points located behind and in the centre-line of rotor at distances 373 m, 499 m and 625 m, respectively. Figure 25 shows the changing wind speed at these points due the frequency support based control strategy. A change in the wind speeds at these points can be noticed a few seconds after the instances of frequency change. The change is smaller in the initial 200 s due to the small changes

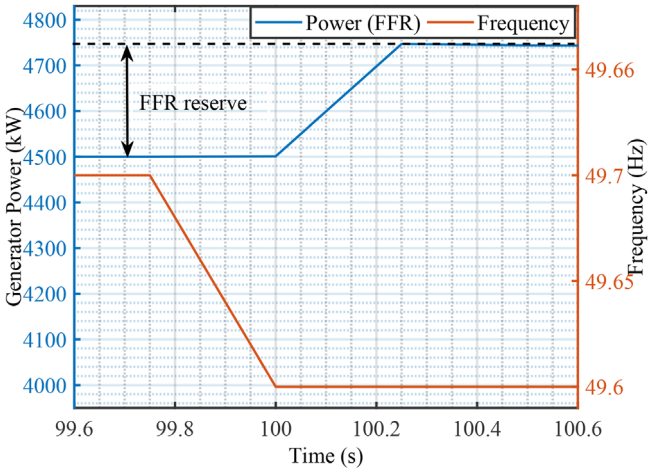

FIGURE 23 FFR Type B service

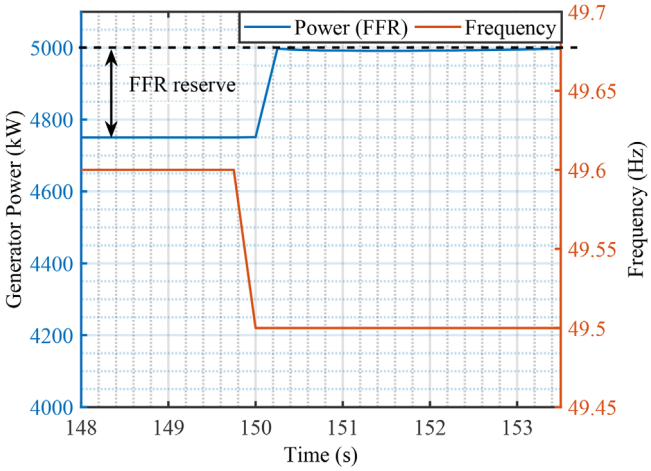

FIGURE 24 FFR Type C service

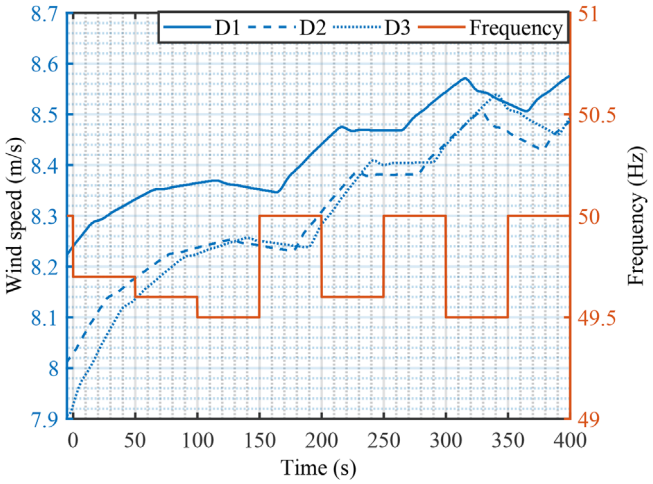

FIGURE 25 Wind speed behind the rotor at 3 different points

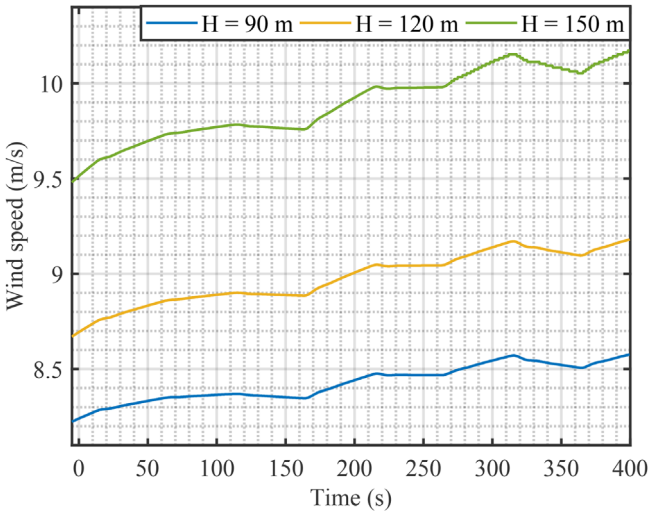

FIGURE 26 Wind speed at different heights behind the rotor

in grid frequency. However, at time t = 200 s, 250 s, 350 s and 400 s, the effect is evident.

In Figure 26, three point at heights of 90 m, 120 m and 150 m are chosen to observe the change in wind speed due to the changing grid speed. Like the previous case, a similar pattern of changing wind speed is observed. These results clearly establish the changing wake effect of a wind turbine providing FFR services.

7 | CONCLUSION

To study the behaviour of the wake behind a wind turbine providing frequency support services, a series of tests are simulated. The NREL 5 MW wind turbine coupled with a PMSG, torque and pitch controller are used to perform these simulations. A modified Jensen wake model that was deemed robust and needful to the simulation designs is used to model the wake behaviour. The simulations are performed for two benchmark ancillary services, that is, 200 mHz symmetrical FCR and FFR, as defined in the ENTSO-E directives. The first frequency dataset used in the analysis is a synthetic sinusoidally varying frequency with varying oscillation periods. This data is used to study the frequency oscillation's replication in the wake behaviour. Second, real grid frequency data from an extreme incidence is used to perform a realistic simulation where the effect of changing grid frequency on the wake can be clearly observable. The simulations are performed for both steady and turbulent wind conditions. The torque control used in the models is designed such that it is capable of following MPPT, PLC as well as grid frequency based deloaded control. The controller is shown to operate with a high tracking performance. Since the simulations include higher wind speed regions, a pitch control system with gain scheduling is also used.

The controller tests performed have strengthened the possibility of an active participation of wind turbines in primary reserve ancillary services. It is clear that the limitations of the wind turbines quick response to the changing grid frequency can be addressed through the development of fast and efficient controllers.

The major topic investigated in this research is to analyse the changes in wake effect of a wind turbine providing frequency support services. The wake effect has been analysed at several locations downwind of the wind turbine. The impact of a changing grid frequency on the nature of the wake is demonstrated. The oscillations in the grid frequency are seen to replicate in the wake behaviour, showing there is a dynamic interaction. Also, changes in the intensity of this effect are clearly visible]with the changing distances behind the wind turbine. It is also observed that the magnitude of frequency support offered by the wind turbine and the slope of the changing grid frequency are also active variables that affect the wake.

The tests presented in this research are performed for a single wind turbine. Therefore, the changes observed in the wake are not extreme. A clear effect of changing grid frequency is however observed. This effect is likely to increase in a high capacity density wind farm where a collective wake effect is generated by several wind turbines. Hence, the main conclusion of this research is that dynamic wake interactions should be taken into account when high density wind farms are to be used to provide dynamic frequency support services such as FCR and FFR.

ACKNOWLEDGEMENTS

This work is supported by the BEOWIND project, funded by the Energy Transition Fund of the Belgian federal government.

CONFLICT OF INTEREST

The authors have declared no conflict of interest.

DATA AVAILABILITY STATEMENT

Data derived from public domain resources.

ORCID

Narender Singh https://orcid.org/0000-0002-0332-8592
Jeroen D. M. De Kooning https://orcid.org/0000-0002-0358-4350
Lieven Vandevelde https://orcid.org/0000-0003-0882-3493

REFERENCES

1. Energy roadmap 2050 Energy. https://ec.europa.eu/energy/
2. Offshore Wind in Europe Key trends and statistics (2019)
3. Global Wind Energy Council: Global wind report 2021. https://gwec.net/wp-content/uploads/2021/03/GWEC-Global-Wind-Report-2021.pdf
4. Technical requirements for the connection of generating stations to the Hydro-Québec transmission system (2019). http://www.hydroquebec.com/
5. Long, Q., Celna, A., Das, K., Sørensen, P.: Fast frequency support from hybrid wind power plants using supercapacitors. Energies 14, 3495 (2021). https://doi.org/10.3390/en14123495
6. Lian, B., Sims, A., Yu, D., Wang, C., Dunn, R.W.: Optimizing lifepo4 battery energy storage systems for frequency response in the UK system. IEEE Trans. Sustain. Energy 8(1), 385–394, (2017). https://doi.org/10.1109/TSTE.2016.2600274
7. Fernandez-Muãoz, D., Guisandez, I., Perez-Diaz, J.I., Chazarra, M., Femandez-Espina, A., Burke, F.: Fast frequency control services in europe. In: 2018 15th International Conference on the European Energy Market (EEM). IEEE, Piscataway (2018). https://doi.org/10.1109/EEM.2018.8469973
8. ENTSO-E.: Survey on ancillary services procurement, balancing market design 2016. https://www.entsoe.eu/publications/market-reports/
9. Singh, N., De Kooning, J.D.M., Vandevelde, L.: Simulation of the primary frequency control pre-qualification test for a 5MW wind turbine. In: IEEE/PES Transmission and Distribution Conference and Exposition (T&D), 2020. https://doi.org/10.1109/TD39804.2020.9299921
10. Daković, J., Ilak, P., Baškarad, T., Krpan, M., Kuzle, I.: Effectiveness of wind turbine fast frequency response control on electrically distanced active power disturbance mitigation. In: Mediterranean Conference on Power Generation, Transmission, Distribution and Energy Conversion (MEDPOWER 2018). IEEE, Piscataway (2018). https://doi.org/10.1049/cp.2018.1923
11. Kim, H., Lee, J., Jang, G., Novel coordinated control strategy of BESS and PMSG-WTG for fast frequency response. Appl. Sci. 11, 3874 (2021). https://doi.org/10.3390/app11093874
12. Zhao, X., Lin, Z., Fu, B., Gong, S.: Research on frequency control method for micro-grid with a hybrid approach of FFR-OPPT and pitch angle of wind turbine. Int. J. Electr. Power Energy Syst. 127, 106670 (2021). ISSN 0142-0615, https://doi.org/10.1016/j.ijepes.2020.106670
13. Heydari, R., Savaghebi, M., Blaabjerg, F.: Fast frequency control of low-inertia hybrid grid utilizing extended virtual synchronous machine. In: 2020 11th Power Electronics, Drive Systems, and Technologies Conference (PEDSTC). IEEE, Piscataway (2020), https://doi.org/10.1109/PEDSTC49159.2020.9088504
14. Rakhshani, E., Torres, J.L.R., Palensky, P., van Meijden, M.d.: Determination of maximum wind power penetration considering wind turbine fast frequency response. In: 2019 IEEE Milan PowerTech. IEEE, Piscataway (2019). https://doi.org/10.1109/PTC.2019.8810492
15. Kayedpour, N., Samani, E.A., De Kooning, J., Vandevelde, L., Crevecoeur, G.: Model predictive control with a cascaded Hammerstein neural network of a wind turbine providing frequency containment reserve. IEEE Trans. Energy Convers. (2021)
16. Singh, N., De Kooning, J.D.M., Vandevelde, L.: Dynamic wake analysis of a wind turbine providing frequency containment reserve in high wind speeds. In: 9th Renewable Power Generation Conference (RPG Dublin Online 2021) 2021. https://doi.org/10.1049/icp.2021.1364
17. Li, S., Haskew, T.A., Swatloski, R.P., Gathings, W.: Optimal and direct-current vector control of direct-driven PMSG wind turbines. IEEE Trans. Power Electron. 27(5), 2325–2337 (2012)
18. Zeng, X., Liu, T., Wang, S., Dong, Y., Chen, Z.: Comprehensive coordinated control strategy of PMSG-based wind turbine for providing frequency regulation services. IEEE Access 7, 63944–63953 (2019)
19. Zhang, Z., Zhao, Y., Qiao, W., Qu, L.: A discrete-time direct torque control for direct-drive PMSG-based wind energy conversion systems. IEEE Trans. Ind. Appl. 51(4), 3504–3514 (2015)
20. Inoue, Y., Morimoto, S., Sanada, M.: Control method for direct torque controlled PMSG in wind power generation system. In: 2009 IEEE International Electric Machines and Drives Conference. IEEE, Piscataway (2009). https://doi.org/10.1109/IEMDC.2009.5075360
21. Abdolghani, N., Milimonfared, J., Gharehpetian, G.B.: A direct torque control method for CSC based PMSG wind energy conversion systems. Renew. Energy Power Quality J. 1(10), 717–723 (2012)
22. Elia: General framework for frequency containment reserve service by non-CIPU resources. https://www.elia.be/
23. Van de Vyver, J., De Kooning, J., Meersman, B., Vandevelde, L., Vandoorn, T.: Droop control as an alternative inertial response strategy for the synthetic inertia on wind turbines. IEEE Trans. Power Syst. 31(2), 1129–1138 (2016)
24. Capacity Densities of European Offshore Wind Farms. Deutsche WindGuard GmbH, Varel (2018). https://vasab.org/document/capacity-densities-of-european-offshore-wind-farms/
25. Lundquist, J.K., DuVivier, K.K., Kaffine, D., et al.: Costs and consequences of wind turbine wake effects arising from uncoordinated wind energy development. Nat Energy 4, 26–34 (2019). doi: s41560-018-0281-2
26. Baker, N., Stanley, A., Thomas, J., Ning, A., Dykes, K.: Best practices for wake model and optimization algorithm selection in wind farm layout optimization. https://www.nrel.gov/docs/fy19osti/72935.pdf

27. Howland, M.F., Lele, S.K., Dabiri, J.O.: Wind farm power optimization through wake steering. Proc. Natl. Acad. Sci. 116(29), 14495–14500 (2019)
28. Kuenzel, S., Kunjumuhammed, L., Pal, B., Erlich, I.: Impact of wakes on wind farm inertial response. In: 2014 IEEE PES General Meeting Conference & Exposition. IEEE, Piscataway (2014)
29. Jonkman, J., Butterfield, S., Musial, W., Scott, G.: Definition of a 5-MW reference wind turbine for offshore system development. https://www.nrel.gov/docs/fy09osti/38060.pdf
30. Jensen, N.O.: A note on wind generator interaction. Risø National Laboratory. Risø-M No. 2411 (1983)
31. Katic, I., Højstrup, J., Jensen, N.O.: A simple model for cluster efficiency. In: Palz, W., Sesto, E. (Eds.) EWEC'86. Proceedings, vol. 1, pp. 407–410. A. Raguzzi, Rome (1987)
32. Elia: General Framework For Frequency Containment Reserve Service by CIPU Technical Units (2019)
33. ENTSO-E.: Technical Requirements for Fast Frequency Reserve Provision in the Nordic Synchronous Area - External document (2021)
34. Elia: grid data overview. https://www.elia.be/en/grid-data
35. ENTSO-E technical report on the January 2019 significant frequency deviations in Continental Europe. https://www.entsoe.eu/news/2019/05/28/entso-e-technical-report-on-the-january-2019-significant-frequency-deviations-in-continental-europe/
36. Højstrup, J.: Velocity spectra in the unstable planetary boundary layer. J. Atmospheric Sci. 39, 2239–2248 (1982)
37. Olesen, H.R., Larsen, S.E., Højstrup, J.: Modeling velocity spectra in the lower part of the planetary boundary layer. Boundary-Layer Meteorol. 29, 285–312 (1984)

How to cite this article: Singh, N., De Kooning, J.D.M., Vandevelde, L.: Dynamic wake analysis of a wind turbine providing frequency support services. IET Renew. Power Gener. 16, 1853–1865 (2022). https://doi.org/10.1049/rpg2.12455